Combined Effect of Shaking Orbit and Vial Orientation on the Agitation-Induced Aggregation of Proteins

Sébastien Dasnoy, Marion Illartin, Julie Queffelec, Aubrey Nkunku, Claude Peerboom

Combined Effect of Shaking Orbit and Vial Orientation on the Agitation-Induced Aggregation of Proteins

Sébastien Dasnoy[a], Marion Illartin[a,b], Julie Queffelec [b], Aubrey Nkunku [c], Claude Peerboom[a]

[a] *UCB Pharma, Chemin du Foriest, 1420 Braine-l'Alleud, Belgium*
[b] *Institut Mines-Télécom (IMT) Mines Albi, Allée des Sciences, 81000 Albi, France*
[c] *ALTEN Belgium, Chaussée de Charleroi 112, 1060 Bruxelles, Belgium*

Orbital shaking in a glass vial is a commonly used forced degradation test to evaluate protein propensity for agitation-induced aggregation. Vial shaking in horizontal orientation has been widely recommended to maximize the air-liquid interface area while ensuring solution contact with the stopper. We evaluated the impact of shaking orbit diameter and frequency, and glass vial orientation (horizontal versus vertical) on the aggregation of three proteins prepared in surfactant-free formulation buffers. As soon as an orbit-specific frequency threshold was reached, an increase in turbidity was observed for the three proteins in vertical orientation only when using a 3 mm agitation orbit, and in horizontal orientation only when using a 30 mm agitation orbit. Orthogonal analyses confirmed turbidity was linked to protein aggregation. The most turbid samples had a visually more homogeneous appearance in vertical than in horizontal orientation, in line with the predicted dispersion of air and liquid phases obtained from computational fluid dynamics agitation simulations. Both shaking orbits were used to assess the performance of nonionic surfactants. We show that the propensity of a protein to aggregate in a vial agitated in horizontal or vertical orientation depends on the shaking orbit, and confirm that Brij® 58 and FM1000 prevent proteins from agitation-induced aggregation at lower concentrations than polysorbate 80.

Introduction

Proteins are used in a wide range of therapeutic applications.[1,2] From manufacturing to patient administration, they can be exposed to various stresses that can impact their stability.[3,4] Protein sensitiv-ity to mechanical stresses is usually evaluated by agitation, free-fall, pumping, or shipment simulations.[5,6] Agitation is a widely used forced degradation approach to evaluate protein propensity for aggregation at air-liquid interfaces[7], which are more detrimental than shear stress.[4,8,9] When in the presence of air-liquid interfaces typically found during filling, transport and compounding operations, proteins can partially unfold and expose their hydrophobic core. The increase of hydrophobic interactions between unfolded proteins can promote the formation of aggregates at the air-liquid interface level, which can then migrate to the solution upon interface renewal,[10-12] and possibly lead to the formation of particles.[13] The presence of aggregates can raise immunogenicity concerns.[14] Several nonionic surfactants and cyclodextrin derivatives have been reported to prevent proteins from aggregation at air-liquid interfaces (Table 1).

Multiple agitation stress settings (e.g., motion type, protein concentration, primary container size and materials of contact, fill and headspace volume, shaking orbit diameter (d) and frequency (f), temperature and light exposure) have been used since no specific guidelines are available to perform agitation studies.[13,15-18] Orbital agitation on a shaking plate has been extensively conducted with samples in horizontal orientation (Table 2), presumably as this allows contact with the stopper and a larger protein exposure to the air-liquid interface area than in vertical orientation.[13,19,20] Increasing the vial fill volume has been shown to limit protein aggregation upon orbital[5] (circular motion) or reciprocating[15] (back-and-forth motion) shaking in horizontal orientation, which supports the critical role of air-liquid interfaces in agitation-induced protein aggregation.[10] The effect of vial orientation has been evaluated in a limited number of orbital shaking studies (f = 200 rpm): Lewis et al[21] reported higher numbers of sub-visible particles (SVP) and visible particles in horizontal than in vertical orientation (d = 19 mm, glass vials), and Wang et al[22] obtained similar aggregation profiles in both horizontal and vertical orientations (d = 15 mm, polypropylene microtubes).

Table 1
Review of excipients used to prevent protein aggregation at air-liquid interface.

Chemical family	Excipient	Efficient concentration (% w/v)	References
Polyoxyethylene sorbitan fatty acid esters	polysorbate 20*	0.001–0.12	15,22,34,38,39,44,48-61
	polysorbate 80*	0.001–0.2	5,6,22,33,44,51,54,56,58-66
Polyoxyethylene-polyoxypropylene block copolymers	poloxamer 188*	0.005–0.1	22,59-62,66-68
	poloxamer 338	0.01	59
	poloxamer 407	0.015–0.2	22,59,67,69
Polyoxyethylene alkyl ethers	Brij® 35	0.005–0.08	22,56,61,62
	Brij® 58	0.0075	43
	Brij® 58 succinate	0.01	70
	polyoxyethylene (9) lauryl ether	0.0075	43
Alcohol ethoxylates	polyoxyl 20 cetostearyl ether	0.01–0.1	59
	Tergitol™ 15-S-15	0.01	59
Cyclodextrin derivatives	hydroxypropyl-β-cyclodextrin*	0.035–10	48,66,67,71,72
	hydroxypropyl-γ-cyclodextrin	0.39–10	67,72
	methyl-β-cyclodextrin	0.033–3.3	72
	dimethyl-β-cyclodextrin	1.3–6.7	71
Sugar-based surfactants	n-dodecyl-β-D-maltoside	0.0075	43
	n-tridecyl-β-D-maltoside	0.0075	43
	6-cyclohexyl-1-hexyl-β-D-maltoside	0.0075	43
	7-cyclohexyl-1-heptyl-β-D-maltoside	0.0075	43
	6-O-monocaprinoyl-α,α-trehalose	0.1	73
	6-O-monolauroyl-α,α-trehalose	0.01–0.1	66,73
	4-n-dodecyl-α,α-trehalose	0.0075	43
	1,2,5,6-tetra-β-D-glucopyranoside-3,4-O-di-tridecyl-D-mannitol	0.0075	43
	sophorolipids (Rewoferm® SL ONE)	0.01	59
Vitamin E-based surfactants	tocofersolan	0.01–0.1	59
	vitamin E 2.2 dimethyl succinate polyethylene glycol 1000	0.04	70
	vitamin E 2.2 dimethyl glutarate polyethylene glycol 1000	0.04	70
Others	FM1000	0.01	44
	polyvinyl alcohol 4-88	0.01–0.1	59
	β-sitosterol methoxypolyethyleneglycol succinate	0.2	70
	Tetronic® 1107	0.01	59
	Triton X-100	0.01–0.08	22,56

* Excipient present in at least one commercial parenteral product.[1,2,74]

Computational fluid dynamics (CFD) simulations of vial orbital shaking in vertical orientation suggest a higher shear rate near the air-liquid interface and a higher air-liquid interface regeneration rate with [d = 4.9 mm, f = 1000 rpm] than with [d = 16 mm, f = 300 rpm] agitation settings.[23]

Most orbital shaking studies (references from Table 2) report the shaking duration and frequency, a parameter that can easily be varied on most commercially available orbital shakers. The shaking orbit is most of the time not explicitly mentioned, probably as it is often a built-in orbital shaker feature that cannot be changed. Both the shaking frequency and orbit contribute to centrifugal acceleration (a_c), which is directly proportional to the centrifugal force as per Newton's second law of motion.

Our objective was to evaluate the impact of shaking orbit and frequency on the aggregation of three proteins stored in surfactant-free formulation buffers, upon agitation in vials held in horizontal or vertical orientation. Protein aggregation was assessed by turbidimetry, nephelometry, dynamic light scattering (DLS), Nile Red fluorescence

Table 2
Review of agitation stress parameters used on a horizontal shaking plate.

Container orientation from the horizontal	Plate Motion	Container
0° (Horizontal)	Orbital	Glass vial[5,19,21,33,37,44,75]
		Polyethylene terephthalate glycol tube[58]
		Polypropylene tube[22,50,51,64,71,76,77]
	Reciprocating	Glass vial[15,16,52,54,59-61,63,65,68,78,79]
	Not reported	Glass vial[32,67]
90° (Vertical)	Orbital	Glass vial[6,21,36,39,55,70,80-82]
	Not reported	Polypropylene tube[22]
30° and 60°	Orbital	Glass vial[43,83]
Not reported	Orbital	Glass vial[21]
		Glass vial[12,34,53,84,85]
		Glass bottle[86]
		Polyethylene terephthalate glycol bottle[35]
		Polypropylene tube[87,88]
	Not reported	Not reported[89]
		Glass vial[56]

spectroscopy, size-exclusion chromatography (SEC), and imaging flow cytometry (IFC). CFD was used to evaluate the impact of orbital shaking settings on the dispersion of air and liquid phases upon agitation, and to calculate the air-liquid interface regeneration rate. The selected agitation conditions were used to assess the performance of four surfactants against protein aggregation.

Materials and Methods

Materials

DIN ISO 2R tubular Type I crimp glass vials (cat. no. 1096873) were purchased from Schott (Mainz, Germany). FluroTec™-laminated 4023/50, B2-40, 13 mm bromobutyl serum stoppers (cat. no. 1358) and 13 mm diameter aluminum overseals with Flip-off® polypropylene disks (cat. no. 5209) were obtained from West Pharmaceutical Services (Exton, PA, United States). Nile Red (Sigma-Aldrich cat. no. 19123), disodium hydrogen phosphate (Na_2HPO_4, Sigma-Aldrich cat. no. S7907), sodium dihydrogen phosphate monohydrate ($NaH_2PO_4 \cdot H_2O$, Sigma-Aldrich cat. no. 71507), sodium chloride (NaCl, Sigma-Aldrich cat. no. S7653), polysorbate 80 (Tween® 80, Sigma-Aldrich cat. no. 59924) and polyethylene glycol hexadecyl ether (Brij® 58, Sigma-Aldrich cat. no. P5884) were supplied by Merck (Darmstadt, Germany). Poloxamer 188 (Kolliphor® P 188 Bio, cat. no. 50424596) and N-myristoyl phenylalanine-N-polyetheramine diamide (FM1000) were gifts from BASF (Ludwigshafen, Germany) and Inter-national Flavors & Fragrances (Wilmington, DE, United States), respectively. Formazin Turbidity standard 4000 NTU (cat. no. 246142) was obtained from Hach (Loveland, CO, United States). Etha-nol absolute (cat. no. 20821.365) and Axygen® AxySeal microplate sealing films (cat. no. PCR-SP) were obtained from Avantor™ (Rad-nor, PA, Unites States). Ultrapure water was obtained from a Milli-Q® IQ 7000 system (cat. no. C189847) equipped with a Millipak® 0.22 μm filter (cat. no. MPGP002A1) from Merck. Prot1, Prot2 and Prot3 are three recombinant proteins of therapeutic interest (various monoclonal antibody formats) manufactured by UCB Pharma (Braine-l'Alleud, Belgium) and stored at a concentration of 100 mg·mL^{-1} in surfactant-free proprietary formulation buffers.

All protein, formulation buffer and surfactant stock solutions were filtered on a polyethersulfone (PES) membrane using a Stericup®(Millipore cat. no. S2GPU02RE) or Steriflip® (Millipore cat. no. SCGP00525) system from Merck. A sufficient volume of surfactant stock solutions was discarded before filtrate collection to allow for filter membrane saturation and ensure reaching the target surfactant concentrations.

Density

Density (ρ) was measured at 20 °C according to the frequency oscillator principle using a density meter (DS7800) from A.KRÜSS Optronic (Hamburg, Germany). The density meter measurement chamber was manually filled using a 2 mL polypropylene syringe (cat. no. 300185) from Becton Dickinson (Franklin Lakes, NJ, United States). The system suitability was checked before use by measuring the density of water at 20 °C (0.9982 ± 0.0005 g·cm^{-3}).

Viscosity

Dynamic viscosity (η) was measured at 20 °C using a rheometer (MCR702e) controlled by the RheoCompass 1.30 software and equipped with a cone-and-plate geometry (CP25-1) from Anton Paar (Graz, Austria). 100 μL of sample were transferred to the rheometer plate. Viscosity was measured at various shear rates ranging from 1 to 20,000 s^{-1}. The measured viscosity values were constant in this shear rate range, which indicates a Newtonian behavior of the three protein solutions. The viscosity value corresponding to a shear rate of 10,000 s^{-1} is reported.

Surface Tensiometry

Surface tension (γ) was measured at 20 °C using a drop shape analyzer (DSA30) controlled by the Advance 1.11 software, with 1 mL disposable syringes (cat. no. SY3601) and dosing needles (cat. no. NE45) from A.KRÜSS Optronic. The measurement duration was 120 s, with an acquisition of one image per second. The surface tension was computed using the Young-Laplace equation, with experimental densities as inputs. The surface tension standard deviation was calculated using 120 images recorded from a single sample.

Agitation

2R vials were filled with 1 mL of protein solution (Prot1, Prot2 or Prot3), stoppered, crimped with aluminum overseals, and packed into 125 × 125 × 45 mm plastic cryoboxes in horizontal (vials on their side separated by tailor-made carton dividers) or vertical (upright vials separated by built-in 7 × 7 dividers) orientation. This fill volume has been recommended for vials of similar dimensions agitated in horizontal orientation on a reciprocating shaker.[16] The boxes were securely tightened to an orbital shaker having a shaking orbit diameter of 3 mm (vibrating platform shaker, Titramax 101 from Heidolph Instruments, Schwabach, Germany) or 30 mm (KS501 from IKA, Staufen, Germany), and a counterclockwise orbital motion. Orbital shaking was conducted over 24 h at a frequency ranging from 300 to 1400 rpm (d = 3 mm) or 150 to 250 rpm (d = 30 mm). The selected frequency values were based on the allowed ranges of orbital shakers, and are aligned with the ranges commonly found in literature (references from Table 2). Independent vials were picked up for analysis at each sampling step. Exposure to light was not controlled.

The angular velocity (ω) was calculated using Eq. 1. a_c was expressed in relative centrifugal force units (RCF) based on Eq. 2, where r is the agitation orbit radius, and g is the gravity of Earth (9.81 m·s^{-2}).

$$\omega = \frac{2\pi f}{60} \quad (1)$$

$$a_c = \frac{r\omega^2}{g} \quad (2)$$

Turbidimetry

The transmitted light intensity is measured with a detector located in front of the incident beam (0° angle). A decrease in light intensity, i.e., an increase in optical density, is due to light scattering as well as potential absorbance from formulation components.[24] Samples (200 μL per well) were filled by reverse pipetting in a 96-well Corning® ultraviolet (UV)-transparent (cat. no. CLS3635) microplate supplied by Merck (Darmstadt, Germany). The plate was sealed and spun for 2 min at 2000 rpm (610 RCF) to remove air bubbles, using a Universal 320R centrifuge from Hettich (Tuttlingen, Germany). The film was removed prior to analysis. Optical density was measured at 350 nm (OD_{350}), at 20 °C, using a Spark® microplate reader controlled by the SparkControl v3.1 software from Tecan (Männedorf, Switzerland). No correction for pathlength was applied. The buffer signal was subtracted.

Nephelometry

The plate prepared for turbidimetry measurements (OD_{350}) was analyzed on a NEPHELOstar Plus microplate-based nephelometer

using the Omega v5.50 (equipment control) and Mars v3.33 (data analysis) softwares from BMG LABTECH (Ortenberg, Germany). The light source wavelength is 635 nm. The forward scattered light between 0 and 80° angles from the incident beam is integrated.[24] The following equipment parameters were used: 1 s time to normalize the results, 1 s measurement interval time, 0.8 s settling time, 50% laser intensity, 2.5 mm beam focus. A linear relationship between results obtained in relative nephelometry units (RNU) and nephelometric turbidity units (NTU) was established in the 0-100 NTU range using Formazin reference suspensions[24,25] prepared by dilution of Formazin 4000 NTU in water: 1 NTU = 3,500 RNU. However, results are reported in RNU as values outside this linearity range (i.e., >350,000 RNU) were obtained.

Dynamic Light Scattering

DLS was used to calculate the hydrodynamic radius (R_h) of spe-cies in solution. Samples were diluted to 1 mg·mL^{-1} in their formu-lation base buffer (buffering species only) and transferred by reverse pipetting (100 μL per well) to a Corning® half-area clear bottom (cat. no. CLS3880) microplate from Merck. The plate was sealed and spun for 2 min at 2000 rpm (610 RCF) to remove air bubbles, using a Universal 320R centrifuge from Hettich. Samples were analyzed at 25 °C using a DynaPro® Plate Reader I controlled by the Dynamics 7.10 software from Wyatt Technology (Santa Barbara, CA, United States). 20 acquisitions of the scattered light intensity fluctuations were recorded over a time interval of 2 s each and averaged. The scattered light intensity decay over time was analyzed by autocorre-lation. The diffusion coefficient was derived from a cumulant fit of the autocorrelation function and used as an input in the Stokes-Ein-stein equation to calculate R_h.

Nile Red Fluorescence Spectroscopy

Nile Red fluorescence spectroscopy was used to probe agitation-induced changes in protein surface hydrophobicity, which can be an indicator of protein unfolding or aggregation.[26] Nile Red crystals were dissolved in ethanol to prepare a solution having an absorbance of 0.22 AU at 552 nm. 95 μL of sample and 5 μL of Nile Red ethanolic solution were added per well in a 384-well black microplate (cat. no. 781209) from Greiner Bio-One (Frickenhausen, Germany). The plate was sealed and spun for 2 min at 2000 rpm (610 RCF) to remove air bubbles, using a Universal 320R centrifuge from Hettich. The film was removed prior to analysis. Nile Red fluorescence emission spec-tra were recorded from 605 to 700 nm, at 20 °C, using a Spark® microplate reader controlled by the SparkControl v3.1 software (Tecan), with an excitation wavelength of 575 nm, a manual gain of 100, an automatic mirror, a Z-position of 20,000 μm, and excitation and emission bandwidths of 5 nm and 20 nm, respectively. The cen-ter of spectral mass (CSM) of each buffer-subtracted emission spec-trum was calculated in Excel® (Microsoft, Redmond, WA, United States) using Eq 3, where λ_i corresponds to an emission wavelength and I_i to the fluorescence intensity at this wavelength.

$$CSM = \frac{\sum_{i=1}^{n} \lambda_i I_i}{\sum_{i=1}^{n} I_i} \quad (3)$$

Size-Exclusion Chromatography

SEC was used to resolve and quantitate protein size variants. A mobile phase (25 mM NaH_2PO_4/Na_2HPO_4, 200 mM NaCl, pH 7.00 ± 0.05) was prepared. The pH of the mobile phase was checked using a Seven Excellence pH meter equipped with an InLab Routine Pro-ISM electrode from Mettler Toledo (Greifensee, Switzerland). The mobile phase was ultrasonicated and vacuum filtered on an Express® PLUS 0.22 μm PES filter (cat. no. GPWP04700) from Merck. Samples where visible particles were detected to the naked eye were centrifuged for 20 min at 4000 RCF using a 5424 R centrifuge from Eppendorf (Hamburg, Germany). Samples were then diluted to a protein concentration of 10 mg·mL^{-1} in the mobile phase and transferred to a Brand® (cat. no. BR781600) microplate from Merck. 4 μL of sample were injected at a flow rate of 0.4 mL·min^{-1} on an Acquity® Ultra Performance Liquid Chromatography (UPLC) H-Class Bio chromatographic system controlled by the Empower™ 3.0 software and equipped with an Ethylene Bridged Hybrid (BEH) SEC column (200 Å pore size, 1.7 μm particle size, 4.6 mm internal diameter, 300 mm length, cat. no. 186005226) and a tunable UV (TUV) detector from Waters (Milford, MA, United States). The column and sample tray temperatures were set to 30 °C and 5 °C, respectively. The detection wavelength was 280 nm. Total high-molecular weight species (HMWS) are reported.

Imaging Flow Cytometry

IFC was used to Quantify SVP.[27] Samples where visible particles were detected to the naked eye were centrifuged for 20 min at 4000 RCF using a 5424 R centrifuge from Eppendorf. 1 μL of 1000X BODIPY™ (PMPBF2) was diluted into 1600 μL of assay buffer kit (cat. no. APH10001) from Luminex (Austin, TX, United States). 1 μL of 1000X ProteoStat® dye was diluted into 1600 μL of assay buffer kit. 1 mL of each diluted dye was added into a 5 mL polypropylene tube, then mixed by vortexing. 80 μL of sample were mixed with 20 μL of the mix of diluted dyes and transferred to a Brand® (cat. no. BR781600) microplate from Merck. Samples were analyzed with a 40x magnification objective using an Amnis® ImageStream$^{®X}$ Mk II imaging flow cytometer calibrated with SpeedBead® reagent (cat. no. 400041) from Luminex. Data were acquired and processed with the INSPIRE™ 201.1 and IDEAS 6.12 softwares (Luminex), respectively. Total SVP counts are reported.

Computational Fluid Dynamics

A CFD modeling approach was followed to simulate the impact of orbital shaking settings on the dispersion of air and liquid phases upon agitation, and to calculate the air-liquid interface regeneration rate,[23] which has been reported as a key contributor to protein aggregation at air-liquid interface.[10]

CFD models were built using the Ansys Fluent 2022 R2 software from Ansys (Canonsburg, PA, United States). The dimensions of the container system, a 2R glass vial closed with a 13 mm serum rubber stopper, were obtained from ISO 8362.[28,29] The vial walls were assumed to be rigid and under no-slip conditions. A vial fill volume of 1 mL was defined, in alignment with the fill volume used for the agitation tests. A mesh was defined for the container system and the liquid phase.

The following air density and viscosity values were obtained from the Fluent software: 1.225 kg·m^{-3} and 1.789 × 10^{-5} kg·m^{-1}·s^{-1}, respectively. The following borosilicate glass density, specific heat and thermal conductivity values were obtained from the Fluent software: 2500 kg·m^{-3}, 840 J·kg^{-1}·K^{-1}, and 0.8 W·m^{-1}·K^{-1}, respectively. The glass properties were used for all container system parts, i.e., the glass vial and the rubber stopper. The diameter of an air bubble in a multi-phase system was obtained from the Fluent software: 8.7 × 10^{-5} m.

The vial orbital motion in the x and y directions was represented in Fluent by a user-defined function written in Python,[30] where $x(t)$ and $y(t)$ represent the vial coordinates (Eq 4), and $v_x(t)$ and $v_y(t)$ rep-resent the vial velocity (Eq 5). The fluid velocity (v) was calculated using Eq 6. The contribution of g was considered in the $-z$ direction.

$$x(t) = r \times cos(2\pi t)$$
$$y(t) = r \times sin(2\pi t) \quad (4)$$

$$v_x(t) = -2\pi r \times sin(\omega t)$$
$$v_y(t) = 2\pi r \times cos(\omega t) \quad (5)$$

$$v = \omega r \quad (6)$$

The liquid phase turbulence associated to a given orbit, frequency and vial orientation was estimated by calculating the Reynolds number (*Re*) using Eq. 7, where ℓ is the characteristic length (container system height in horizontal orientation, and diameter in vertical orientation).

$$Re = \frac{\rho v \ell}{\eta} \quad (7)$$

Phase exchanges between immiscible fluids were simulated using the Volume of Fluid (VOF) model while the phase change and wall adhesion were not considered. The anti-diffusion effect was applied on the system to have a sharp interface between the air and the solu-tion. Since the volume fraction (*F*) between air and liquid phases ranges from 0.0 (air) to 1.0 (liquid), an iso-surface was created to gen-erate the air-liquid interface, where $F = 0.5$ for all elements. VOF results were considered as convergent if the relative errors of resid-uals were lower than 10^{-2}. The mean flow characteristics were esti-
mated using a standard k-ε turbulence model which is suitable for multiphase fluid flows with small pressure gradients and high *Re* shear stresses. The Ansys Fluent SIMPLEC algorithm was selected as a pressure-velocity coupling solution method, with a pressure-correction under-relaxation factor of 1.0.

The pressure, velocity and continuity equations were solved in the allocated cells every 0.1 s. The number of iterations was defined from the elapsed time to obtain a stable drag coefficient (C_D), which indicates the system has reached a steady state.

The air-liquid interface regeneration rate (G) is a numerical method used in Fluent to track the interface between two immiscible fluid phases in a two-phase fluid simulation. It determines how quickly the simula-tion updates the position and shape of the interface and is influenced by various factors such as the fluid properties, flow conditions, turbulence models, and mesh resolution. The air-liquid interface generation rate in a mesh cell (G_c) was calculated using Eq. 8, where U_n is the fluid axial velocity normal to the interface, i.e., the inflow of fluid to the mesh cell, A_0 is the interface area in the mesh cell, V_c is the volume of the mesh cell, and $(\nabla \cdot \vec{U})_f$ represents the velocity vector divergence along x, y and z directions for a wetted cell, i.e. the change of fluid volume in the mesh cell. U_n, V_c and $(\nabla \cdot \vec{U})_f$ values were computed in Fluent at the mesh face center level and extracted using the "*xy* plot" for each mesh along the surface representing the air-liquid interface. Computed values were then exported to Excel® for calculating G_c and G values. G results from the integration of positive G_c values over all mesh cells where air-liquid interface is present (Eq. 9), and represents the volume of fluid per unit time ($mL \cdot s^{-1}$) reaching the layer of mesh cells containing air-liquid interface.[23]

$$G_c = \frac{U_n A_0}{V_c} + \left(\nabla \cdot \vec{U}\right)_f \quad (8)$$

$$G = \sum_{i=1}^{n} G_{ci} F_i V_{ci} \quad (9)$$

Data Visualization

Graphs were created with Prism 8.1 (GraphPad Software, San Diego, CA, United States).

Results

Physical Properties of Protein Solutions

The density, viscosity, and surface tension values of the three 100 $mg \cdot mL^{-1}$ protein solutions were determined (Table 3). Prot3 had a higher density, a lower viscosity, and a lower surface tension than Prot2 and Prot1. Prot2 had a higher viscosity than Prot1. The density and surface tension values of Prot1 and Prot2 were similar. A slight opalescence was noticed for Prot1 only.

Agitation

The 100 $mg \cdot mL^{-1}$ protein solutions were agitated for 24 h in vials held in horizontal or vertical orientation, using various shaking orbit diameter and agitation frequency setting combinations. Samples were analyzed by turbidimetry (Fig. 1). For each orbit value, no change in turbidity was observed after 24 h of agitation using the lowest frequency value (i.e., [d = 3 mm, f = 300 rpm, a_c = 0.2 RCF] and [d = 30 mm, f = 150 rpm, a_c = 0.4 RCF]). An increase in turbidity with agitation time (t) was observed for the three proteins, either in verti-cal orientation only for d = 3 mm ($f \geq 800$ rpm, $a_c \geq 1.1$ RCF), or in horizontal orientation only for d = 30 mm ($f \geq 200$ rpm, $a_c \geq 0.7$ RCF). The [d = 3 mm, f = 800 rpm, vertical] agitation settings led to a visu-ally more homogeneous liquid phase than the [d = 30 mm, f = 200 rpm, vertical] agitation settings, where floating visible par-ticles were observed for the three proteins, as illustrated for Prot1 in Fig. 2. Prot1 sedimentation was observed after post-agitation storage at 2–8 °C of [d = 3 mm, f = 800 rpm, vertical] samples (Fig. 3). The shaking orbit-dependent effect of vial orientation initially observed at 100 $mg \cdot mL^{-1}$ (Fig. 1) was confirmed for the three proteins diluted to concentrations as low as 1 $mg \cdot mL^{-1}$ in their formulation buffers (Fig. 4). The agitation-induced increase in turbidity between 20 $mg \cdot mL^{-1}$ and 100 $mg \cdot mL^{-1}$ was of the same order of magnitude for Prot2 and Prot3.

Computational Fluid Dynamics

A mesh was defined by dividing the container system into 57,399 cells, 261,521 faces and 164,867 nodes (Fig. 5A). 85% of the system mesh elements had an orthogonal quality of 92%. 95% of the mesh cells had the same area. The container system inner volume esti-mated by Fluent was 4110 mm^3. The 100 $mg \cdot mL^{-1}$ Prot1 solution was selected as a model liquid for CFD simulations as it led to the largest increase in turbidity upon agitation (Figs. 1 and 4). The Prot1 liquid density, dynamic viscosity, and surface tension values were obtained from Table 3. The 1 mL fill volume (1000 mm^3) corresponds to a liquid height of 4.97 mm (13,295 cells) in vertical orientation, assuming a cylindrical shape (flat meniscus), and to 4.26 mm (17,300 cells) in horizontal orientation (Fig. 5A).

CFD simulations of the four orbital shaking settings illustrated in Fig. 2 were run. The pressure, velocity and continuity equations were solved every 0.1 s in the allocated cells. A stable C_D value was reached after around 4 s for each set of orbital shaking parameters, both in

Table 3
Physical properties of the 100 $mg \cdot mL^{-1}$ proteins. Density and viscosity values provide from single measurements. Surface tension values provide from 120 images recorded from a single sample.

Protein	Density (ρ, $g \cdot cm^{-3}$)	Dynamic viscosity (η, mPa·s)	Surface tension (γ, $mN \cdot m^{-1}$)
Prot1	1.036	4.1	59.82 ± 0.38
Prot2	1.037	6.3	60.02 ± 0.48
Prot3	1.040	3.0	57.02 ± 0.41

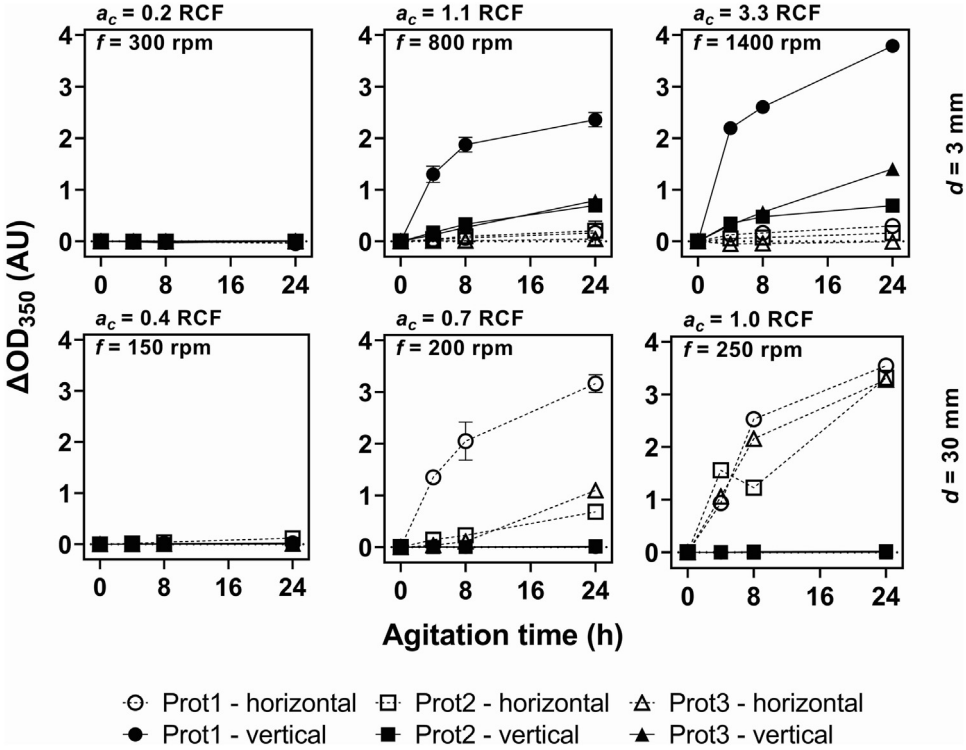

Figure 1. Evolution of turbidity with agitation time using various shaking orbit diameter (d) and frequency (f) setting combinations. The turbidity difference from unagitated sample (ΔOD_{350}) is reported. Vials were filled with 1 mL of 100 mg·mL^{-1} protein solution and agitated in vertical or horizontal orientation. Results provide from a minimum of two replicate measurements. Error bars represent one standard deviation and may be not apparent in case they are smaller than symbols.

vertical and horizontal orientation. Since 100 iterations were defined per time step, a total of 4000 iterations was performed per agitation condition. Computed values were calculated from a steady-state situation, i.e., after around 4 s in vertical or horizontal position. A homogeneous dispersion of liquid and air phases at steady state was

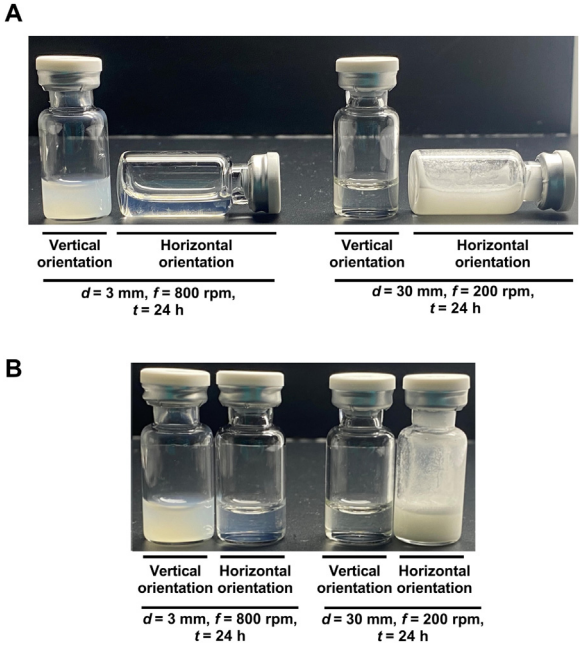

Figure 2. Visual aspect of vials filled with 1 mL of 100 mg·mL^{-1} Prot1 solution and agitated for 24 h in vertical or horizontal orientation using two shaking orbit diameter (d) and frequency (f) setting combinations. Two illustrations of the same samples are provided: (A) vials pictured in the orientation used during agitation tests, (B) vials pictured in upright position.

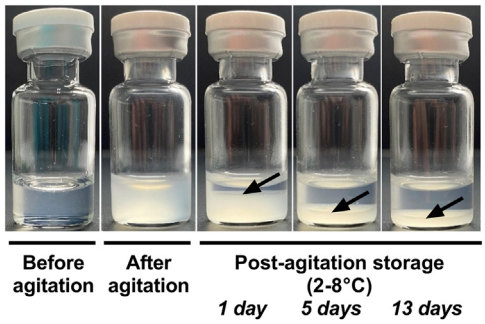

Figure 3. Visual aspect of vials filled with 1 mL of 100 mg·mL^{-1} Prot1 solution before agitation, after 24 h of agitation at 800 rpm on a 3 mm diameter orbital shaker in vertical orientation, and post-agitation quiescent storage at 2-8 °C in vertical orientation. Arrows indicate the location of the sedimentation front.

predicted for the [d = 3 mm, f = 800 rpm, vertical] condition, where the liquid phase remains close to the vial walls. Other agitation conditions led to a more heterogeneous distribution of liquid and air phases, where the liquid phase moves back and forth from one vial side to the other (Fig. 5B). G_c values were mainly driven by the velocity vector divergence term $(\nabla \cdot \vec{U})_f$.

Larger Re values were obtained for [d = 30 mm, f = 200 rpm] than for [d = 3 mm, f = 800 rpm] agitation conditions. Larger Re (due to larger $\nearrow$ values) and G values were obtained in horizontal than in ver-tical orientation (Table 4).

Characterization of Aggregate Species

Samples from the three 100 mg·mL^{-1} protein solutions agitated for 24 h using Fig. 2 orbital shaking settings were analyzed using a range of orthogonal analytical techniques, as no single analytical

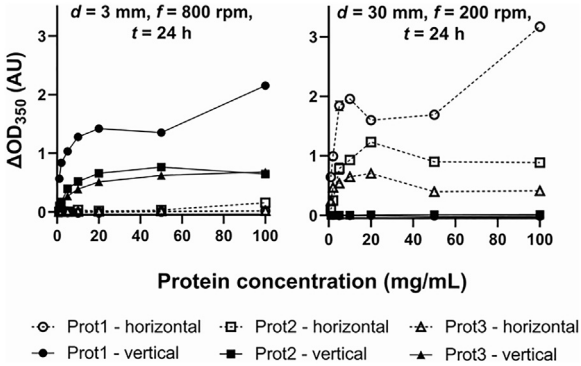

Figure 4. Evolution of turbidity with protein concentration using two shaking orbit diameter (d) and frequency (f) setting combinations. The turbidity difference from unagitated sample (ΔOD_{350}) is reported. Vials were filled with 1 mL of protein solution and agitated for 24 h in vertical or horizontal orientation. Results provide from four replicate measurements. Error bars represent one standard deviation and may be not apparent in case they are smaller than symbols.

method covers all protein aggregation stages and aggregate sizes.[4,15,31]

Non-separation methods were used for quantifying turbidity (turbidimetry and nephelometry), getting a qualitative indication of changes in protein surface hydrophobicity (Nile Red fluorescence spectroscopy), and providing a size distribution profile of aggregates in the nanometer to micrometer range (DLS). Agitation-induced increases in turbidity detected by turbidimetry (Fig. 6A) were also detected by nephelometry (Fig. 6B) – except for the [Prot1, d = 30 mm, f = 200 rpm, horizontal] samples. In addition, the highest post-agitation OD_{350} values (Fig. 6A) were associated to an increase in polydispersity (i.e., multimodal distributions – data not shown) and R_h by DLS (Fig. 6C), and a Nile Red CSM position shift towards shorter wavelengths (blue shift, Fig. 6D).

Separation methods were used for quantifying HMWS (SEC) and SVP (IFC). An increase in OD_{350} (Fig. 6A) corresponds to an increase in HMWS (Fig. 6E) – except for the [Prot3, d = 3 mm, f = 800 rpm, vertical] samples, and to an increase in total SVP counts – except for the [Prot1, d = 30 mm, f = 200 rpm, horizontal] samples (Fig. 6F). Higher SVP counts tagged by both Proteostat® and BODIPY™ dyes were also detected in [d = 3 mm, f = 800 rpm, horizontal] samples while no agita-tion-induced protein aggregation was detected by the other methods.

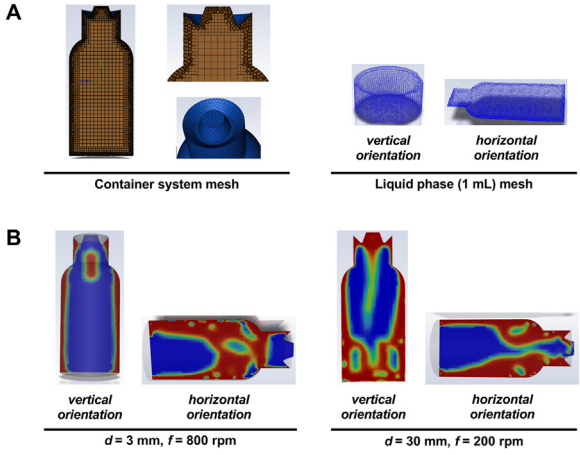

Figure 5. CFD simulation results for vials filled with 1 mL of Prot1 solution and agitated in vertical or horizontal orientation using two shaking orbit diameter (d) and frequency (f) setting combinations: (A) container system and liquid phase mesh, (B) liquid (red color) and air (blue color) volume fractions at steady state.

Table 4
CFD simulation results: Reynolds number (Re) and air-liquid interface regeneration rates (G) values calculated from various orbital shaking parameters.

Agitation settings	Vial orientation	Re	G (mL·s^{-1})
d = 3 mm, f = 800 rpm	Horizontal	429	0.29
	Vertical	254	0.08
d = 30 mm, f = 200 rpm	Horizontal	1072	0.65
	Vertical	635	0.09

Effect of Surfactants

A 50 mg·mL^{-1} Prot1 solution was agitated over 24 h in the presence of polysorbate 80, poloxamer 188, Brij® 58 or FM1000, using the orbital shaking settings illustrated in Fig. 2. Both agitation settings allowed evaluating the effect of surfactant nature and concentration on Prot1 aggregation (Fig. 7). Prot1 agitation-induced aggregation using the most stringent agitation settings by turbidimetry (d = 30 mm, f = 200 rpm, horizontal) was inhibited in the presence of surfactant concentrations (% w/v) larger than or equal to 0.5×10^{-3} for both Brij® 58 or FM1000, 1×10^{-3} for poloxamer 188, and 2×10^{-3} for polysorbate 80. No clear differences between Brij® 58, FM1000 and poloxamer 188 were observed using the less stringent agitation settings (d = 3 mm, f = 800 rpm, vertical).

Discussion

For each shaking orbit, the absence of increase in turbidity at low shaking frequency (Fig. 1, [d = 3 mm, f = 300 rpm] and [d = 30 mm, f = 150 rpm]) supports that a minimum a_c value is required to trigger protein aggregation.[16] Increasing the shaking frequency led to an increase in turbidity values[32-34], but only in orbit-specific vial orientations: [d = 3 mm, $f \geq$ 800 rpm, vertical] and [d = 30 mm, $f \geq$ 200 rpm, horizontal] (Fig. 1). Therefore, a_c values originating from different shaking orbits in a given vial orientation cannot be used to compare agitation-induced protein aggregation data.

Turbidity values reflect a higher propensity of Prot1 for agitation-induced aggregation as compared to Prot2 and Prot3 (Figs. 1 and 4), which illustrates that the propensity to aggregate at the air-liquid interface depends on the protein properties.[35-38] Agitated Prot2 and Prot3 samples led to similar increases in turbidity from 20 mg·mL^{-1} to 100 mg·mL^{-1} (Fig. 4), which supports the fact that increasing the concentration of a protein may limit its propensity for agitation-induced aggregation[39], possibly by decreasing the surface tension, modifying the glass wall wetting properties and therefore the air-liquid interface size.[16]

Both microplate-based turbidimetry and nephelometry methods were used to measure sample turbidity. Larger differences between unagitated and agitated samples were detected by nephelometry (Fig. 6B) than by turbidimetry (Fig. 6A). Nephelometry is in theory more sensitive than optical density because it measures scattered light while turbidimetry measures transmitted light.[24] However, the nephelometry settings we used did not allow detecting turbidity in the most turbid sample (Prot1, d = 30 mm, f = 200 rpm, horizontal), probably because of light blockage. Therefore, both techniques provide complementary information as nephelometry and turbidimetry are more sensitive to low and high turbidity samples, respectively.

The higher R_h values measured by DLS (Fig. 6C) and the blue shift in CSM from Nile Red fluorescence emission spectra (Fig. 6D) sup-ports the presence of aggregates in turbid samples but may not be comparable to non-turbid samples in case of differences in protein concentration[40,41] due to sample heterogeneity. No protein concentration data are reported as highly turbid samples led to inconsistent results by UV absorption spectroscopy at 280 nm, even after light scattering signal subtraction.

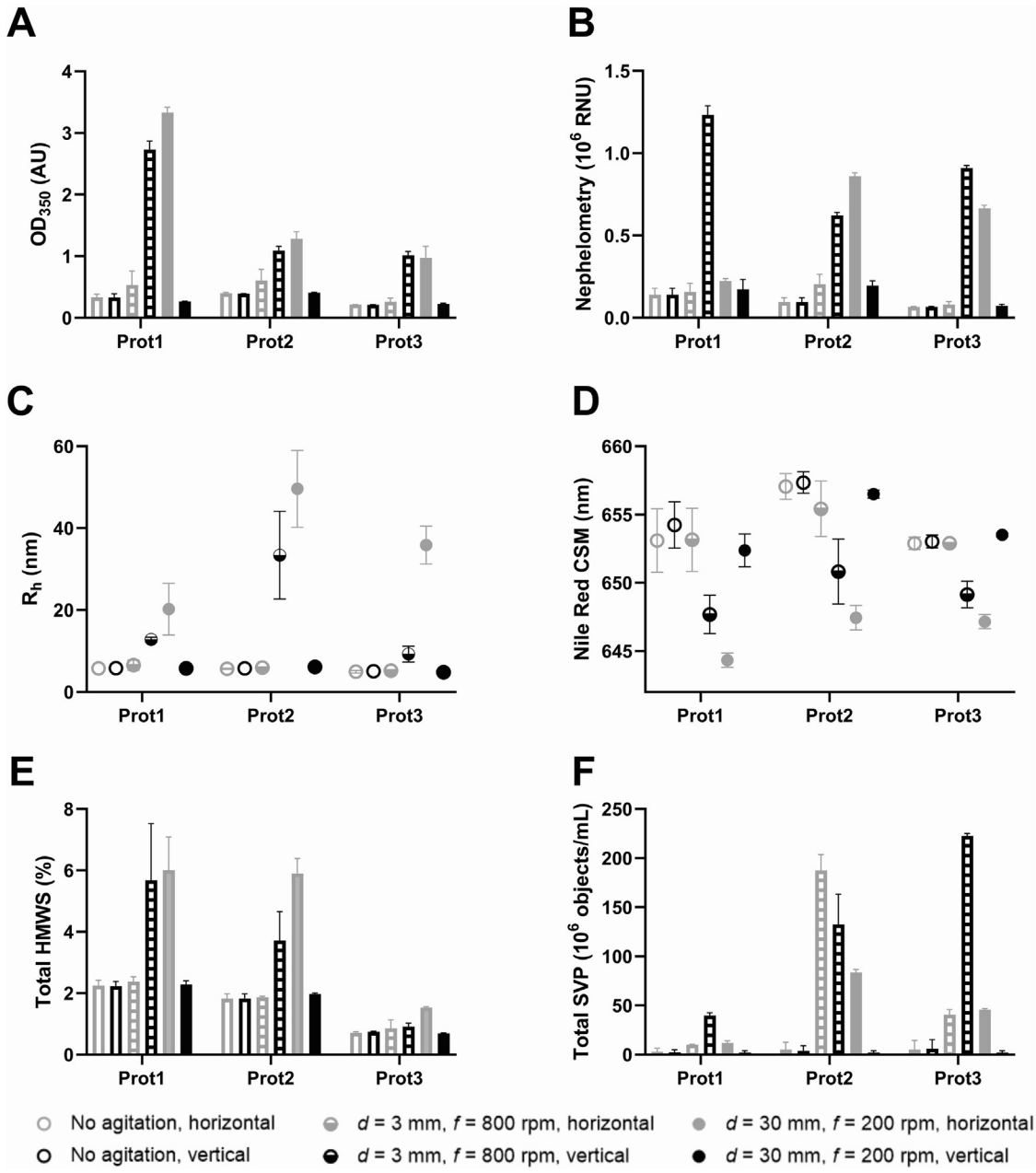

Figure 6. Effect of agitation on turbidity by (A) turbidimetry and (B) nephelometry, (C) R_h, (D) Nile Red CSM, (E) total HMWS, and (F) total SVP. Vials were filled with 1 mL of 100 mg·mL^{-1} protein solution and agitated for 24 h in vertical or horizontal orientation, using two shaking orbit diameter (d) and frequency (f) setting combinations. Results provide from a minimum of two independent measurements. Error bars represent one standard deviation and may be not apparent in case they are smaller than symbols.

Separation techniques also showed some limitations in the analysis of high turbidity samples, as large particles could possibly not be detected by SEC[4] (HMWS, Fig. 6E) or IFC (SVP, Fig. 6F), due to pre-analysis centrifugation or to size limitations inherent to the method (maximum 450 kDa for the SEC column and 60 μm for the IFC magnification objective).

An increase in SVP counts was obtained for Prot2 and Prot3 upon agitation in horizontal position, whatever the agitation orbit (Fig. 6F). This could be due to solution contact with stopper coating materials,[42] and as such supports the general recommendation to conduct agitation studies in vials held in horizontal orientation.[13,19,20]

CFD simulations predicted a more homogeneous distribution of the air and liquid phases in the [d = 3 mm, f = 800 rpm, vertical] than in the [d = 30 mm, f = 200 rpm, horizontal] agitations conditions (Fig. 5). This prediction was confirmed by a visually more homogeneous appearance of all aggregated protein solutions in the former than in the latter case, as illustrated for the 100 mg·mL^{-1} Prot1 solution (Fig. 2). A lower turbulence (lower *Re* value, Table 4) and a more symmetrical container system in vertical than in horizontal orientation can contribute to getting a higher homogeneity.

CFD simulations did not show a link between agitation parameters and the propensity of Prot1 to aggregate in a specific vial orientation. While air-liquid interface regeneration rate has been reported to be a key contributor to protein aggregation at the air-liquid interface,[10-12] vial orientations leading to protein aggregation (i.e.,[d = 3 mm, f = 800 rpm, vertical] and [d = 30 mm, f = 200 rpm, hori-zontal], Figs. 1 and 4) do not correspond to the highest G values for each set of agitation parameters (Table 4). Our [d = 3 mm, f = 800

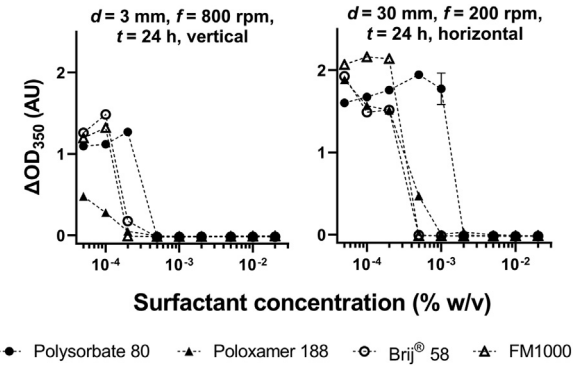

Figure 7. Evolution of turbidity with surfactant concentration using two shaking orbit diameter (d), frequency (f) and vial orientation setting combinations. The turbidity difference from unagitated sample (ΔOD_{350}) is reported. Vials were filled with 1 mL of 50 mg·mL^{-1} protein solution and agitated for 24 h. Results provide from four replicate measurements. Error bars represent one standard deviation and may be not apparent in case they are smaller than symbols.

rpm] and [d = 30 mm, f = 200 rpm] agitation conditions led to similar G values in vertical orientation, whereas higher G values were reported with [d = 4.9 mm, f = 1000 rpm] than [d = 16 mm, f = 300 rpm] agitation parameters, for a vial of similar dimensions and fill volume agitated in vertical orientation.[23] G was not an appropriate predictor of protein propensity for aggregation in the agitation conditions used in our study, as G_c values were mainly driven by the velocity vector divergence term $(\nabla \cdot \vec{U})_f$, which constantly reaches a high value in case the liquid can easily escape the vial walls.

The two orbital shaking settings allowed a comparison of the performance of four surfactants in their ability to protect Prot1 from agitation-induced aggregation (Fig. 7) and confirm the previously reported performance of Brij® 58[43] and FM1000[44] at lower concentrations than polysorbate 80. Based on the most discriminant agitation conditions in terms of turbidity (d = 30 mm, f = 200 rpm, horizontal), the minimum surfactant concentration (% w/v) to prevent aggregation was lower for Brij® 58 (0.5×10^{-3}) and FM1000 (0.5×10^{-3}) than for poloxamer 188 (1.0×10^{-3}) and polysorbate 80 (2.0×10^{-3}). These concentrations are larger than or in the same order of magnitude as some critical micelle concentration (CMC) val-ues (% w/v) reported in literature (FM1000[44]: 0.055×10^{-3}, Brij® 58[43] and poloxamer 188[44]: 0.6×10^{-3}, polysorbate 80[45]: 1.6×10^{-3}), and could support that the minimum surfactant concentration to be added in a protein formulation needs to be larger than or equal to its CMC value[3], as for polysorbates in most commercial monoclonal anti-body drug products.[2] However, the diversity of surfactant grades and CMC determination methods lead to a wide range of reported CMC values,[46,47] making the use of CMC values challenging to support the definition of a surfactant concentration.

The orbital shaking conditions used in this study allow assessing protein propensity for aggregation at air-liquid interface and evaluating the performance of excipients. However, the use of multiple mechanical stresses is recommended to define the surfactant concentration to be added in a protein formulation.[5,6,19]

Conclusion

Since aggregation was observed in vertical orientation only when using a 3 mm agitation orbit, and in horizontal orientation only when using a 30 mm agitation orbit, the impact of vial orientation on the agitation-induced aggregation of proteins depends on the shaking orbit. However, this work does not allow predicting the impact of vial orientation on protein aggregation using other agitation orbits than 3 mm and 30 mm. The dispersion of air and liquid phases predicted by CFD agitation simulations reflected the visual homogeneity of aggregated samples. Both agitation settings allowed evaluating the performance of excipients against agitation-induced aggregation. Brij® 58 and FM1000 prevented proteins from agitation-induced aggregation at lower concentrations than polysorbate 80, which could possibly be an advantage from a toxicological and economic standpoint. These results suggest that not all orbital shakers are capable of triggering protein aggregation in a vial held in horizontal orientation, which is a widely recommended approach in terms of contact with stopper and air-liquid interface area.

Declaration of Competing Interest

The authors declare that they have no known competing financial interests or personal relationships that could have appeared to influence the work reported in this paper.

CRediT authorship contribution statement

Sébastien Dasnoy: Conceptualization, Formal analysis, Investigation, Methodology, Supervision, Validation, Visualization, Writing – original draft, Writing – review & editing. **Marion Illartin:** Conceptualization, Investigation, Methodology, Validation, Writing – review & editing. **Julie Queffelec:** Conceptualization, Investigation, Methodology, Validation, Writing – review & editing. **Aubrey Nkunku:** Formal analysis, Software, Visualization, Writing – review & editing. **Claude Peerboom:** Resources.

Acknowledgements

The authors thank Sabrina Di Tore, Chaimaa Hidan and Mélanie Leemans for analytical support. Critical manuscript review by Audrey Arrighi, Egon Deyaert, James Heads and Jan Massant is gratefully acknowledged.

References

1. Gervasi V, Dall Agnol R, Cullen S, McCoy T, Vucen S, Crean A. Parenteral protein formulations: an overview of approved products within the European Union. *Eur J Pharm Biopharm*. 2018;131:8–24.
2. Strickley RG, Lambert WJ. A review of formulations of commercially available antibodies. *J Pharm Sci*. 2021;110(7):2590–2608.
3. Manning MC, Liu J, Li T, Holcomb RE. Rational design of liquid formulations of proteins. *Adv Protein Chem Struct Biol*. 2018;112:1–59.
4. Wang W, Roberts CJ. Protein aggregation - Mechanisms, detection, and control. *Int J Pharm*. 2018;550(1-2):251–268.
5. Torisu T, Maruno T, Hamaji Y, Ohkubo T, Uchiyama S. Synergistic effect of cavitation and agitation on protein aggregation. *J Pharm Sci*. 2017;106(2):521–529.
6. Grabarek AD, Bozic U, Rousel J, et al. What makes polysorbate functional? Impact of polysorbate 80 grade and quality on IgG stability during mechanical stress. *J Pharm Sci*. 2020;109(1):871–880.
7. Nowak C, K Cheung J, M Dellatore S, et al. Forced degradation of recombinant monoclonal antibodies. *MAbs*. 2017;9(8):1217–1230.
8. Maa YF, Hsu CC. Protein denaturation by combined effect of shear and air-liquid interface. *Biotechnol Bioeng*. 1997;54(6):503–512.
9. Mahler H-C, Fischer S, Randolph TW, Carpenter JF. Protein aggregation and particle formation: effects of formulation, interfaces, and drug product manufacturing operations. In: Wang W, Roberts CJ, eds. *Aggregation of Therapeutic Proteins*. Hoboken, NJ: John Wiley & Sons, Inc.; 2010:301–331.
10. Li J, Krause ME, Chen X, et al. Interfacial stress in the development of biologics: fundamental understanding, current practice, and future perspective. *AAPS J*. 2019;21(3):44.
11. Ghazvini S, Kalonia C, Volkin DB, Dhar P. Evaluating the role of the air-solution interface on the mechanism of subvisible particle formation caused by mechanical agitation for an IgG1 mAb. *J Pharm Sci*. 2016;105(5):1643–1656.
12. Koepf E, Eisele S, Schroeder R, Brezesinski G, Friess W. Notorious but not understood: how liquid-air interfacial stress triggers protein aggregation. *Int J Pharm*. 2018;537(1-2):202–212.
13. Halley J, Chou YR, Cicchino C, et al. An industry perspective on forced degradation studies of biopharmaceuticals: survey outcome and recommendations. *J Pharm Sci*. 2020;109(1):6–21.
14. Rosenberg AS. Effects of protein aggregates. *AAPS J*. 2006;8(3):E501–E507.

15. Kiese S, Pappenberger A, Friess W, Mahler H-C. Shaken, not stirred: mechanical stress testing of an IgG1 antibody. *J Pharm Sci*. 2008;97(10):4347–4366.
16. Eppler A, Weigandt M, Hanefeld A, Bunjes H. Relevant shaking stress conditions for antibody preformulation development. *Eur J Pharm Biopharm*. 2010;74(2):139–147.
17. Hawe A, Wiggenhorn M, van de Weert M, Garbe JHO, Mahler H-C, Jiskoot W. Forced degradation of therapeutic proteins. *J Pharm Sci*. 2012;101(3):895–913.
18. Tamizi E, Jouyban A. Forced degradation studies of biopharmaceuticals. *Eur J Pharm Biopharm*. 2016;98:26–46.
19. Fleischman ML, Chung J, Paul EP, Lewus RA. Shipping-induced aggregation in therapeutic antibodies: utilization of a scale-down model to assess degradation in monoclonal antibodies. *J Pharm Sci*. 2017;106(4):994–1000.
20. Kizuki S, Wang Z, Torisu T, Yamauchi S, Uchiyama S. Relationship between aggregation of therapeutic proteins and agitation parameters. *J Pharm Sci*. 2023;112 (2):492–505.
21. Lewis LM, Pizzo ME, Sinha S, Ahmed SS, Joseph L. Visible and sub-visible particle formation for a model bioconjugate. *AAPS PharmSciTech*. 2017;18(3):926–931.
22. Wang S, Wu G, Zhang X, Tian Z, Zhang N, Hu T, Dai W, Qian F. Stabilizing two IgG1 monoclonal antibodies by surfactants. *Eur J Pharm Biopharm*. 2017;114:263–277.
23. Bai G, Bee JS, Biddlecombe JG, Chen Q, Leach WT. Computational fluid dynamics (CFD) insights into agitation stress methods in biopharmaceutical development. *Int J Pharm*. 2012;423(2):264–280.
24. Kunz P, Stuckenberger E, Hausmann K, et al. Understanding opalescence measurements of biologics - a comparison study of methods, standards, and molecules. *Int J Pharm*. 2022;628: 122321.
25. Barros M, Zhang X, Kenrick S, Valente JJ. Opalescence measurements: improvements in fundamental knowledge, identifying sources of analytical biases, and advanced applications for the development of therapeutic proteins. *J Pharm Sci*. 2021;110(11):3550–3557.
26. Hawe A, Sutter M, Jiskoot W. Extrinsic fluorescent dyes as tools for protein characterization. *Pharm Res*. 2008;25(7):1487–1499.
27. Probst C. Characterization of protein aggregates, silicone oil droplets, and protein-silicone interactions using imaging flow cytometry. *J Pharm Sci*. 2020;109(1):364–374.
28. International Organization for Standardization. *ISO 8362-1 - Injection Containers and Accessories – Part 1: Injection Vials Made of Glass Tubing*. 2018. Geneva, Switzerland.
29. International Organization for Standardization. *ISO 8362-2 - Injection Containers and Accessories – Part 2: Closures for Injection Vials*. 2015. Geneva, Switzerland.
30. Python Software Foundation. *The Python Language Reference (v3.9)*. 2020. https://www.python.org/.
31. den Engelsman J, Garidel P, Smulders R, et al. Strategies for the assessment of protein aggregates in pharmaceutical biotech product development. *Pharm Res*. 2011;28(4):920–933.
32. Sluzky V, Tamada JA, Klibanov AM, Langer R. Kinetics of insulin aggregation in aqueous solutions upon agitation in the presence of hydrophobic surfaces. *Proc Natl Acad Sci U S A*.. 1991;88(21):9377–9381.
33. Kerwin BA, Akers MJ, Apostol I, et al. Acute and long-term stability studies of deoxy hemoglobin and characterization of ascorbate-induced modifications. *J Pharm Sci*. 1999;88(1):79–88.
34. Thirumangalathu R, Krishnan S, Ricci MS, Brems DN, Randolph TW, Carpenter JF. Silicone oil- and agitation-induced aggregation of a monoclonal antibody in aqueous solution. *J Pharm Sci*. 2009;98(9):3167–3181.
35. Simler BR, Hui G, Dahl JE, Perez-Ramirez B. Mechanistic complexity of subvisible particle formation. *J Pharm Sci*. 2012;101(11):4140–4154.
36. Jayaraman M, Buck PM, Ignatius AA, King KR, Wang W. Agitation-induced aggregation and subvisible particulate formation in model proteins. *Eur J Pharm Biopharm*. 2014;87(2):299–309.
37. Shieh IC, Patel AR. Predicting the agitation-induced aggregation of monoclonal antibodies using surface tensiometry. *Mol Pharm*. 2015;12(9):3184–3193.
38. Gamage CLD, Weis DD, Walters BT. Identification of agitation-induced unfolding events causing aggregation of monoclonal antibodies using hydrogen exchange-mass spectrometry. *J Pharm Sci*. 2022;111(8):2210-2216..
39. Treuheit MJ, Kosky AA, Brems DN. Inverse relationship of protein concentration and aggregation. *Pharm Res*. 2002;19(4):511–516.
40. Stetefeld J, McKenna SA, Patel TR. Dynamic light scattering: a practical guide and applications in biomedical sciences. *Biophys Rev*. 2016;8(4):409–427.
41. Ota C, Tanaka SI, Takano K. Revisiting the Rate-Limiting Step of the ANS-Protein Binding at the Protein Surface and Inside the Hydrophobic Cavity. *Molecules*. 2021;26(2).
42. Teska BM, Brake JM, Tronto GS, Carpenter JF. Aggregation and particle formation of therapeutic proteins in contact with a novel fluoropolymer surface versus siliconized surfaces: effects of agitation in vials and in prefilled syringes. *J Pharm Sci*. 2016;105(7):2053–2065.
43. Yue L, Yan Z, Li H, Liu X, Sun P. Brij-58, a potential injectable protein-stabilizer used in therapeutic protein formulation. *Eur J Pharm Biopharm*. 2020;146:73–83.
44. Katz JS, Nolin A, Yezer BA, Jordan S. Dynamic properties of novel excipient suggest mechanism for improved performance in liquid stabilization of protein biologics. *Mol Pharm*. 2019;16(1):282–291.
45. Wan LS, Lee PF. CMC of polysorbates. *J Pharm Sci*. 1974;63(1):136–137.
46. Bollenbach L, Buske J, Mäder K, Garidel P. Poloxamer 188 as surfactant in biological formulations - an alternative for polysorbate 20/80? *Int J Pharm*. 2022;620: 121706.
47. Smith OEP, Waters LJ, Small W, Mellor S. CMC determination using isothermal titration calorimetry for five industrially significant non-ionic surfactants. *Colloids Surf B Biointerfaces*. 2022;211: 112320.
48. Charman SA, Mason KL, Charman WN. Techniques for assessing the effects of pharmaceutical excipients on the aggregation of porcine growth hormone. *Pharm Res*. 1993;10(7):954–962.
49. Bam NB, Cleland JL, Yang J, Manning MC, Carpenter JF, Kelley RF, Randolph TW. Tween protects recombinant human growth hormone against agitation-induced damage via hydrophobic interactions. *J Pharm Sci*. 1998;87(12):1554–1559.
50. Kreilgaard L, Jones LS, Randolph TW, Frokjaer S, Flink JM, Manning MC, Carpenter JF. Effect of Tween 20 on freeze-thawing- and agitation-induced aggregation of recombinant human factor XIII. *J Pharm Sci*. 1998;87(12):1597–1603.
51. Chou DK, Krishnamurthy R, Randolph TW, Carpenter JF, Manning MC. Effects of Tween 20 and Tween 80 on the stability of albutropin during agitation. *J Pharm Sci*. 2005;94(6):1368–1381.
52. Mahler H-C, Senner F, Maeder K, Mueller R. Surface activity of a monoclonal antibody. *J Pharm Sci*. 2009;98(12):4525–4533.
53. Brych SR, Gokarn YR, Hultgen H, Stevenson RJ, Rajan R, Matsumura M. Characterization of antibody aggregation: role of buried, unpaired cysteines in particle formation. *J Pharm Sci*. 2010;99(2):764–781.
54. Kishore RSK, Kiese S, Fischer S, Pappenberger A, Grauschopf U, Mahler H-C. The degradation of polysorbates 20 and 80 and its potential impact on the stability of biotherapeutics. *Pharm Res*.. 2011;28(5):1194–1210.
55. Basu P, Krishnan S, Thirumangalathu R, Randolph TW, Carpenter JF. IgG1 aggregation and particle formation induced by silicone-water interfaces on siliconized borosilicate glass beads: a model for siliconized primary containers. *J Pharm Sci*. 2013;102(3):852–865.
56. Agarkhed M, O'Dell C, Hsieh M-C, Zhang J, Goldstein J, Srivastava A. Effect of surfactants on mechanical, thermal, and photostability of a monoclonal antibody. *AAPS PharmSciTech*. 2018;19(1):79–92.
57. Gandhi AV, Randolph TW, Carpenter JF. Conjugation of emtansine onto trastuzumab promotes aggregation of the antibody-drug conjugate by reducing repulsive electrostatic interactions and increasing hydrophobic interactions. *J Pharm Sci*. 2019;108(6):1973–1983.
58. Doshi N, Giddings J, Luis L, et al. A comprehensive assessment of all-oleate polysorbate 80: free fatty acid particle formation, interfacial protection and oxidative degradation. *Pharm Res*. 2021;38(3):531–548.
59. Heitz M., Khan T., Kientz H.S., Müller C., Pfaff J.M. 2021. Alternative surfactants as stabilizers for therapeutic formulations. WO2022008468A1.
60. Johann F, Wöll S, Winzer M, Snell J, Valldorf B, Gieseler H. Miniaturized forced degradation of therapeutic proteins and ADCs by agitation-induced aggregation using orbital shaking of microplates. *J Pharm Sci*. 2022;111(5):1401–1413.
61. Zürcher D, Caduff S, Aurand L, Capasso Palmiero U, Wuchner K, Arosio P. Comparison of the protective effect of polysorbates, poloxamer and brij on antibody stability against different interfaces. *J Pharm Sci*. 2023. S0022-3549(23)00231-9.
62. Katakam M, Bell LN, Banga AK. Effect of surfactants on the physical stability of recombinant human growth hormone. *J Pharm Sci*. 1995;84(6):713–716.
63. Mahler H-C, Müller R, Friess W, Delille A, Matheus S. Induction and analysis of aggregates in a liquid IgG1-antibody formulation. *Eur J Pharm Biopharm*. 2005;59(3):407–417.
64. Wang W, Wang YJ, Wang DQ. Dual effects of Tween 80 on protein stability. *Int J Pharm*. 2008;347(1-2):31–38.
65. Larson NR, Wei Y, Prajapati I, et al. Comparison of polysorbate 80 hydrolysis and oxidation on the aggregation of a monoclonal antibody. *J Pharm Sci*. 2020;109 (1):633–639.
66. Zoeller MP, Hafiz S, Marx A, Erwin N, Fricker G, Carpenter JF. Exploring the protein stabilizing capability of surfactants against agitation stress and the underlying mechanisms. *J Pharm Sci*. 2022;111(12):3261–3274.
67. Dasnoy S, Dezutter N, Lemoine D, Le Bras V, Préat V. High-throughput screening of excipients intended to prevent antigen aggregation at air-liquid interface. *Pharm Res*. 2011;28(7):1591–1605.
68. Grapentin C, Müller C, Kishore RSK, et al. Protein-polydimethylsiloxane particles in liquid vial monoclonal antibody formulations containing poloxamer 188. *J Pharm Sci*. 2020;109(8):2393–2404.
69. Katakam M, Banga AK. Use of poloxamer polymers to stabilize recombinant human growth hormone against various processing stresses. *Pharm Dev Technol*. 1997;2 (2):143–149.
70. Brosig S, Cucuzza S, Serno T, et al. Not the usual suspects: alternative surfactants for biopharmaceuticals. *ACS Appl Mater Interfaces*. 2023;15(29):34540–34553.
71. Tavornvipas S, Tajiri S, Hirayama F, Arima H, Uekama K. Effects of hydrophilic cyclodextrins on aggregation of recombinant human growth hormone. *Pharm Res*. 2004;21(12):2369–2376.
72. Serno T, Carpenter JF, Randolph TW, Winter G. Inhibition of agitation-induced aggregation of an IgG-antibody by hydroxypropyl-beta-cyclodextrin. *J Pharm Sci*. 2010;99(3):1193–1206.
73. Schiefelbein L, Keller M, Weissmann F, Luber M, Bracher F, Friess W. Synthesis, characterization and assessment of suitability of trehalose fatty acid esters as alternatives for polysorbates in protein formulation. *Eur J Pharm Biopharm*. 2010;76 (3):342–350.
74. Food and Drugs Administration (FDA). Inactive Ingredients Database. Accessed on 21 July 2023. https://www.fda.gov/drugs/drug-approvals-and-databases/inactive-ingredients-database-download.
75. Witeof AE, Daniels AL, Rea LT, et al. Machine learning and accelerated stress approaches to differentiate potential causes of aggregation in polyclonal antibody formulations during shipping. *J Pharm Sci*. 2021;110(7):2743–2752.
76. Cordes AA, Carpenter JF, Randolph TW. Accelerated stability studies of abatacept formulations: comparison of freeze-thawing- and agitation-induced stresses. *J Pharm Sci*. 2012;101(7):2307–2315.

77. Liu L, Randolph TW, Carpenter JF. Particles shed from syringe filters and their effects on agitation-induced protein aggregation. *J Pharm Sci*. 2012;101(8):2952–2959.
78. Kiese S, Pappenberger A, Friess W, Mahler H-C. Equilibrium studies of protein aggregates and homogeneous nucleation in protein formulation. *J Pharm Sci*. 2010;99(2):632–644.
79. Kalonia C, Kumru OS, Kim JH, Middaugh CR, Volkin DB. Radar chart array analysis to visualize effects of formulation variables on IgG1 particle formation as measured by multiple analytical techniques. *J Pharm Sci*. 2013;102(12):4256–4267.
80. Fesinmeyer RM, Hogan S, Saluja A, et al. Effect of ions on agitation- and temperature-induced aggregation reactions of antibodies. *Pharm Res*. 2009;26(4):903–913.
81. Joubert MK, Luo Q, Nashed-Samuel Y, Wypych J, Narhi LO. Classification and characterization of therapeutic antibody aggregates. *J Biol Chem*. 2011;286(28):25118–25133.
82. Kopp MRG, Wolf Pérez A-M, Zucca MV, et al. An accelerated surface-mediated stress assay of antibody instability for developability studies. *MAbs*. 2020;12(1):1815995.
83. Fang W-J, Ingle RG, Liu J-W, Ge X-Z, Wang H. Freeze-dried monoclonal antibody formulations are unexpectedly more prone to degradation than liquid formulations under shaking stress. *J Pharm Sci*. 2022;111(7):2134–2138.
84. Telikepalli SN, Kumru OS, Kalonia C, et al. Structural characterization of IgG1 mAb aggregates and particles generated under various stress conditions. *J Pharm Sci*. 2014;103(3):796–809.
85. Koepf E, Schroeder R, Brezesinski G, Friess W. The missing piece in the puzzle: prediction of aggregation via the protein-protein interaction parameter A(∗)(2). *Eur J Pharm Biopharm*. 2018;128:200–209.
86. Vidanovic D, Milic Askrabic J, Stankovic M, Poprzen V. Effects of nonionic surfactants on the physical stability of immunoglobulin G in aqueous solution during mechanical agitation. *Pharmazie*. 2003;58(6):399–404.
87. Macchi F, Hoffmann SV, Carlsen M, et al. Mechanical stress affects glucagon fibrillation kinetics and fibril structure. *Langmuir*. 2011;27(20):12539–12549.
88. Gerhardt A, Bonam K, Bee JS, Carpenter JF, Randolph TW. Ionic strength affects tertiary structure and aggregation propensity of a monoclonal antibody adsorbed to silicone oil-water interfaces. *J Pharm Sci*. 2013;102(2):429–440.
89. Kwon YM, Baudys M, Knutson K, Kim SW. In situ study of insulin aggregation induced by water-organic solvent interface. *Pharm Res*. 2001;18(12):1754–1759.